Available online at www.sciencedirect.com
SCIENCE DIRECT®
European Journal of Mechanics B/Fluids 25 (2006) 95–112

Observations on the predictions of fully developed rotating pipe flow using differential and explicit algebraic Reynolds stress models

Olof Grundestam [a,*], Stefan Wallin [a,b], Arne V. Johansson [a]

[a] *Department of Mechanics, Royal Institute of Technology, KTH, SE-100 44 Stockholm, Sweden*
[b] *Aeronautics Division, FFA, Swedish Defence Research Agency (FOI), SE-172 90 Stockholm, Sweden*

Received 21 September 2004; received in revised form 17 February 2005; accepted 24 March 2005

Available online 28 April 2005

Abstract

The differences between two differential Reynolds stress models (DRSM) and their corresponding explicit algebraic Reynolds stress models (EARSM) are investigated by studying fully developed axially rotating turbulent pipe flow. The mean flow and the turbulence quantities are strongly influenced by the imposed rotation, and is well captured by the differential models as well as their algebraic truncations. All the tested models give mean velocity profiles that are in good qualitative agreement with the experimental data. It is demonstrated that the predicted turbulence kinetic energy levels vary dramatically depending on the diffusion model used, and that this is closely related to the model for the evolution of the length-scale determining quantity. Furthermore, the effect of the weak equilibrium assumption, underlying the EARSMs, and the approximation imposed for 3D mean flows on the turbulence levels are investigated. In general the predictions obtained with the EARSMs rather closely follow those of the corresponding DRSMs.

Keywords: Rotating pipe flow; Swirling flow; Reynolds stress turbulence model

1. Introduction

Fully developed axially rotating pipe flow is an often used test case for turbulence models. The unintuitive deviation from a solid body rotation in the fully developed state can be ascribed to an intricate influence of, and interaction between, the Reynolds stress components. The prediction of the resulting effects of the axial rotation is a difficult challenge for engineering type of turbulence models. The standard K–ε and K–ω two-equation models are essentially unsensitive to rotation and are therefore unable to capture the phenomena that are characteristic to rotating pipe flow such as a parabolic-like azimuthal velocity profile and an increasingly laminar-like axial velocity profile for increasing rate of rotation. Models based on the transport equation of the Reynolds stresses offer a choice where more flow physics such as rotation can be included in a natural way.

Fully developed *rotating* pipe flow constitutes, by definition, a 3D mean flow. This can be seen by forming the invariants of the mean velocity gradients. For a 2D mean flow, e.g. *nonrotating* pipe flow, there are two independent invariants while for a

* Corresponding author.
E-mail addresses: olof@mech.kth.se (O. Grundestam), stefan.wallin@foi.se (S. Wallin), viktor@mech.kth.se (A.V. Johansson).

0997-7546/$ – see front matter
doi:10.1016/j.euromechflu.2005.03.004

3D mean flow there are up to five, three for this particular case. In this sense the 3D character of the mean flow is continuously governed by one parameter only, the axial rotation rate of the pipe. The 3D effects can therefore be made gradually more important by increasing the rotation rate. The dependence on one spatial coordinate only, makes the numerical implementation relatively simple.

Related studies of interest include a recent study of Jakirlić et al. [1] in which a number of models are tested for different rotating and swirling flows. Fu et al. [2] performed a comparative study of the performance of different modelling approaches for axisymmetric turbulent shear flows with and without swirl. Hirai et al. [3] studied the laminariztion phenomena in an axialy rotating pipe flow. Pettersson et al. [4] investigated the performance of linear and nonlinear Reynolds stress transport models in conjunction with the relaxation approach of Durbin [5]. Wallin and Johansson [6] discussed the mechanism behind the parabolic shape of the azimuthal velocity profile in relation to EARSM predictions. Direct numerical simulations have been performed by for instance Eggels et al. [7] and Orlandi and Fatica [8]. Imao et al. [9] studied fully developed rotating pipe flow experimentally and Facciolo [10] has presented a recent experimental study that also includes the swirling jet. Oberlack [11] analyses fully developed pipe flow by using symmetry methods. In a recent study by Jakirlić and Hanjalić [12], a model for the turbulence kinetic energy and stress dissipation was proposed. The performance of this model was evaluated for e.g. rotating pipe flow.

An explicit algebraic Reynolds stress model (EARSM) is the result of a formal approximation of a full differential Reynolds stress model (DRSM) in the weak equilibrium limit. The resulting constitutive relation is used together with a two-equation platform, in this case the K–ω model. The aim with the present study is to investigate how the differences between an EARSM and a DRSM affect the flow predictions. One of the main focus points of the present paper is to increase the understanding of how the two platform equations interact and also how the EARSM assumptions affect the predictions. The scrutiny of this problem is an important step on the way towards better two-equation platforms, for EARSMs.

Four different models have been tested, the EARSM by Wallin and Johansson [6] (WJ-EARSM), the extension of the WJ-EARSM to nonlinear pressure strain rate models proposed by Grundestam et al. [13] (GWJ-EARSM) and the corresponding DRSMs denoted L-DRSM and NL-DRSM, respectively. This means that the calibrated EARSM-parameter values have been applied to the corresponding DRSM without any recalibration. The "log-layer" was, however, still in good agreement with the DNS data by Alvelius and Johansson [14] for nonrotating channel flow at $Re_\tau = u_\tau h/\nu = 180$ where h is the half channel width. For the DRSM-computations, the ω-equation has been used to determine the lengthscale, and for the EARSM, the standard high-Re K–ω equations have been used as model platform. Thus, the EARSM and DRSM should be as comparable as possible.

2. Governing equations

Fully developed rotating pipe flow is a 3D mean flow which is dependent on one spatial coordinate only, r, in a cylindrical coordinate system (r, θ, z). The mean velocity flow field is constrained to the axial and azimuthal directions. The radial mean velocity is zero in the fully developed state. The Reynolds averaged Navier Stokes equations for the azimuthal and axial mean velocities are given by

$$\frac{\partial U_\theta}{\partial t} = \frac{1}{r^2}\frac{\partial}{\partial r}\left[r^3 \nu \frac{\partial}{\partial r}\left(\frac{U_\theta}{r}\right) - r^2 \overline{u_r u}_\theta\right], \tag{1}$$

$$\frac{\partial U_z}{\partial t} = -\frac{1}{\rho}\frac{\partial P}{\partial z} + \frac{1}{r}\frac{\partial}{\partial r}\left[\nu r \frac{\partial U_z}{\partial r} - r\overline{u_r u}_z\right]. \tag{2}$$

The components of the Reynolds stress tensor are given by their transport equation which in a Cartesian coordinate system can be written as

$$\frac{D\overline{u_i u_j}}{Dt} = \mathcal{P}_{ij} - \varepsilon_{ij} + \Pi_{ij} + \mathcal{D}_{ij} \tag{3}$$

where $\mathcal{P}_{ij}$ is the production, ε_{ij} the dissipation rate tensor, Π_{ij} the pressure strain rate tensor and $\mathcal{D}_{ij}$ the diffusion of the Reynolds stresses. $D/Dt = \partial/\partial t + U_k \partial/\partial x_k$ is the advection by the mean flow.

In (3) and in the auxiliary lengthscale-determining equation (e.g. the ω-equation (9)), all the quantities except the production of the Reynolds stresses, $\mathcal{P}_{ij}$, have to be modelled. The production can be expressed explicitly in terms of the strain and rotation rate tensors

$$S_{ij} = \frac{1}{2}\left(\frac{\partial U_i}{\partial x_j} + \frac{\partial U_j}{\partial x_i}\right) \Omega_{ij} = \frac{1}{2}\left(\frac{\partial U_i}{\partial x_j} - \frac{\partial U_j}{\partial x_i}\right) \tag{4}$$

and the Reynolds stress tensor. In both the DRSM and, in particular, the EARSM formulation the Reynolds stress anisotropy tensor plays a fundamental role. It is defined as

$$a_{ij} = \frac{\overline{u_i u_j}}{K} - \frac{2}{3}\delta_{ij} \tag{5}$$

where $K = \frac{1}{2}\overline{u_i u_i}$ is the turbulence kinetic energy. We may utilize these quantities to express the production tensor as

$$\boldsymbol{\mathcal{P}} = K\left(-\frac{4}{3}\mathbf{S} - (\mathbf{aS} + \mathbf{Sa}) + \mathbf{a}\boldsymbol{\Omega} - \boldsymbol{\Omega}\mathbf{a}\right). \tag{6}$$

A matrix notation is used in (6), where e.g. **aS** has the components $a_{ik}S_{kj}$. For rotating pipe flow, the mean strain and rotation rate tensors evaluated in a nonrotating frame of reference, read

$$\mathbf{S} = \frac{1}{2}\begin{bmatrix} 0 & \frac{\mathrm{d}U_\theta}{\mathrm{d}r} - \frac{U_\theta}{r} & \frac{\mathrm{d}U_z}{\mathrm{d}r} \\ \frac{\mathrm{d}U_\theta}{\mathrm{d}r} - \frac{U_\theta}{r} & 0 & 0 \\ \frac{\mathrm{d}U_z}{\mathrm{d}r} & 0 & 0 \end{bmatrix}, \tag{7}$$

$$\boldsymbol{\Omega} = \frac{1}{2}\begin{bmatrix} 0 & -\frac{\mathrm{d}U_\theta}{\mathrm{d}r} - \frac{U_\theta}{r} & -\frac{\mathrm{d}U_z}{\mathrm{d}r} \\ \frac{\mathrm{d}U_\theta}{\mathrm{d}r} + \frac{U_\theta}{r} & 0 & 0 \\ \frac{\mathrm{d}U_z}{\mathrm{d}r} & 0 & 0 \end{bmatrix}. \tag{8}$$

Since the problem is formulated in a nonrotating frame of reference the effect of rotation enters only through the boundary conditions on the azimuthal mean velocity. Thus, no Coriolis term appears in (3) and $\boldsymbol{\Omega}$ has no explicit dependency on the angular velocity of the pipe.

We here choose $\omega = \varepsilon/(\beta^* K)$ ($\beta^* = 0.09$) as the lengthscale determining quantity. The modelled transport equation for ω reads

$$\frac{\partial \omega}{\partial t} = \alpha\frac{\omega}{K}\mathcal{P} - \beta\omega^2 + \mathcal{D}_\omega \tag{9}$$

where $\mathcal{P} = \mathcal{P}_{ii}/2$ is the production of turbulence kinetic energy and $\mathcal{D}_\omega$ the diffusion of ω. $\alpha = 5/9$ and $\beta = 3/40$ are model constants, see Wilcox [15].

In the EARSM computations, relation (3) is replaced with its trace, the transport equation for the turbulence kinetic energy, K, that reads

$$\frac{DK}{Dt} = \mathcal{P} - \varepsilon + \mathcal{D}_K \tag{10}$$

(where D_K is the diffusion of K and ε is the dissipation rate) together with an explicit relation between the Reynolds stress anisotropy tensor and the mean strain and rotation rate tensors normalized with the turbulence timescale, $\tau = K/\varepsilon$, $a_{ij} = a_{ij}(\tau\mathbf{S}, \tau\boldsymbol{\Omega})$, see Appendix A. All equations are integrated down to the wall.

2.1. Modelling

To close the system of equations, the unknown quantities Π_{ij}, ε_{ij}, $\mathcal{D}_{ij}$, $\mathcal{P}_\omega$, $\mathcal{D}_{ij}$, $\mathcal{D}_K$ and $\mathcal{D}_\omega$ have to be modelled in terms of the known quantities S_{ij}, Ω_{ij}, $\overline{u_i u_j}$ and ω.

It is convenient to lump the pressure strain rate and the dissipation rate anisotropy models together since the slow pressure strain and the dissipation rate anisotropy, $e_{ij} = \varepsilon_{ij}/\varepsilon - 2/3\delta_{ij}$, tensors are modelled in principally the same way. The complete model that is quasilinear in the Reynolds stress anisotropy tensor reads

$$\frac{\boldsymbol{\Pi}}{\varepsilon} - \mathbf{e} = -\frac{1}{2}\left(C_1^0 + C_1^1\frac{\mathcal{P}}{\varepsilon}\right)\mathbf{a} + \frac{K}{\varepsilon}\left(C_2\mathbf{S} + \frac{C_3}{2}\left(\mathbf{aS} + \mathbf{Sa} - \frac{2}{3}\{\mathbf{aS}\}\mathbf{I}\right) - \frac{C_4}{2}(\mathbf{a}\boldsymbol{\Omega} - \boldsymbol{\Omega}\mathbf{a}) + C_\Omega\left(\mathbf{N}^\Omega + \mathbf{N}^S\right)\right) \tag{11}$$

where {} denotes the trace and **I** is the identity matrix. The term quasilinear here signifies that only a scalar nonlinearity in the anisotropy is allowed. This enters through the inclusion of $\mathcal{P}/\varepsilon \equiv -\tau\{\mathbf{aS}\}$. In (11) we have also included the last term that represents an extension that is nonlinear in the mean strain and rotation rate tensors,

$$\mathbf{N}^\Omega = \frac{1}{\sqrt{-II_\Omega}}\left(\mathbf{a}\boldsymbol{\Omega}^2 + \boldsymbol{\Omega}^2\mathbf{a} - \frac{2}{3}\{\mathbf{a}\boldsymbol{\Omega}^2\}\mathbf{I}\right), \tag{12}$$

$$\mathbf{N}^S = \frac{1}{\sqrt{II_S}}\left(\mathbf{aS}^2 + \mathbf{S}^2\mathbf{a} - \frac{2}{3}\{\mathbf{aS}^2\}\mathbf{I}\right). \tag{13}$$

$\mathbf{N}^{\Omega}$ and $\mathbf{N}^{S}$ were originally proposed by Sjögren and Johansson [16] and the inclusion of these terms were shown to improve predictions in strongly rotating generic flows. By using the same coefficient in front of both (12) and (13) the total contribution vanishes in parallel flows. The L-DRSM corresponds to $C_{\Omega} = 0$, while for the NL-DRSM $C_{\Omega} = 0.5$, which is the value suggested by Sjögren and Johansson [16].

The diffusion of the Reynolds stresses can schematically be written as

$$\mathcal{D}_{ij} = -\frac{\partial}{\partial x_m}\left(J_{ijm} - \nu\frac{\partial \overline{u_i u_j}}{\partial x_m}\right) \tag{14}$$

where J_{ijm} depends on correlations of the fluctuating velocity and pressure and thus needs to be modelled. In the present DRSM computations the diffusion model by Daly and Harlow, [17], has been adopted. In Cartesian tensor notation the Daly and Harlow model reads

$$J_{ijk} = -c_s\frac{K}{\varepsilon}\overline{u_k u_l}\frac{\partial \overline{u_i u_j}}{\partial x_l}. \tag{15}$$

In a cylindrical coordinate system the model expression is somewhat lengthy and is therefore given in Appendix B. For the EARSMs the diffusion of the Reynolds stress anisotropy is neglected due to the weak equilibrium assumption proposed by Rodi [18]. However, the diffusion of K and ω are accounted for in the respective platform equations by using the diffusion model by Daly and Harlow [17]. The effect of using a simpler effective eddy-viscosity diffusion approach is also investigated. The implications are discussed in Section 6.

The Daly and Harlow model for ω reads

$$\mathcal{D}_{\omega} = \frac{1}{r}\frac{\partial}{\partial r}\left[r\left(\nu + c_{\omega}\frac{K}{\varepsilon}\overline{u_r u_r}\right)\frac{\partial \omega}{\partial r}\right] \tag{16}$$

and correspondingly for K (with c_{ω} replaced by c_s). The model parameters used are $c_s = c_{\omega} = 0.11$ for the L-DRSM and the EARSMs and $c_s = c_{\omega} = 0.08$ for the NL-DRSM. c_s and c_{ω} have been calibrated by considering the log-layer of nonrotating channel flow.

Two EARSM formulations have been used, the formulation proposed by Wallin and Johansson [6] and its extension to a nonlinear pressure strain rate model, see Grundestam et al. [13]. Both of these formulations use a complete five element tensor basis for 3D mean flows such that

$$\mathbf{a} = \sum_{i=1,3,4,6,9} \beta_i \mathbf{T}^{(i)}. \tag{17}$$

The β-coefficients are explicitly dependent on the production to dissipation ratio, $\mathcal{P}/\varepsilon$. The consistency condition $\mathcal{P}/\varepsilon \equiv \tau\{\mathbf{aS}\}$ results in a cubic equation for 2D mean flows (see Appendix A). Normally, this would also be used as an approximation in 3D mean flows. A more accurate approximation for 3D cases was derived by Wallin and Johansson [6]. This approximation will be used for the highest rate of rotation case studied here, where the large deviation from a 2D state turns out to require this 3D corrected description for convergence of the solution. See Appendix A for a brief summary.

The curvature correction proposed by Wallin and Johansson [19] has been used in conjunction with both explicit models. This contribution is derived from the advection of the Reynolds stress anisotropy and can be written as

$$-\tau\left(\mathbf{a}\boldsymbol{\Omega}^{(r)} - \boldsymbol{\Omega}^{(r)}\mathbf{a}\right) \tag{18}$$

where τ is the turbulence timescale. Adding (18) to the algebraic approximation of the transport equation for a_{ij} yields a systematic improvement of the weak equilibrium assumption in that it gives an approximation of the neglection of the advection of a_{ij} in a local streamline-based system. For fully developed rotating pipe flow, the correction exactly represents the advection and can be written

$$\Omega^{(r)}_{ij} = -\epsilon_{ij3}\frac{U_{\theta}}{r} \tag{19}$$

For an EARSM using a pressure strain rate model linear in $\boldsymbol{\Omega}$, $C_{\Omega} = 0$ in (11), the correction (18) can easily be included through the transformation

$$\boldsymbol{\Omega} \to \boldsymbol{\Omega}^{*} = \boldsymbol{\Omega} - \frac{1}{A_0}\boldsymbol{\Omega}^{(r)}, \quad A_0 = \frac{C_4}{2} - 1. \tag{20}$$

For a nonlinear pressure strain rate model, $C_{\Omega} \neq 0$, the amount of algebra generated for 3D mean flows makes the exact EARSM formulation somewhat awkward. A discussion on this and suggested approximations can be found in Grundestam et al. [20].

3. Numerical procedure

Since fully developed rotating (and nonrotating) pipe flow is dependent on one spatial coordinate only, the flow can be computed using a special code developed for problems with dependence on one spatial dimension, see Wallin and Mårtensson [21]. For the spatial discretization a second order central difference scheme is used. The time stepping towards a steady state is done with the implicit Euler backward step method. The corresponding system matrix is inverted by an iterative method for each timestep.

To reach the desired Reynolds number based on the mean bulk velocity and the pipe diameter, the pressure gradient, $\partial P/\partial z$, is set appropriately. In order to keep the Reynolds number constant when rotation is applied to the pipe, the pressure gradient is adjusted accordingly.

The system of governing equations is solved in the nonrotating system meaning that the azimuthal velocity is nonzero on the wall. The equivalent alternative would have been to solve the problem in a rotating frame by including the appropriate terms associated with system rotation and imposing a zero velocity on the wall.

The grid used is a one dimensional stretched grid from the center of the pipe to the pipe wall. The stretch factor is 0.96 and the number of grid points is 100 with a concentration of points near the wall. To get an indication of grid dependence, a grid with 400 points and a stretch factor of 0.99 was tested. The model predictions were, however, virtually unaffected.

4. Results

The fully developed rotating pipe flow was computed for three rotation numbers $Ro = U_\theta(R)/U_m = 0$, 0.5 and 1 and a Reynolds number based on the pipe diameter and the mean bulk velocity of $Re = U_m D/\nu = 20\,000$. The results can be seen in Fig. 1–4. As comparison, the experimental results by Imao et al. [9] are shown in the corresponding figures. A lower Reynolds number, $Re = 4900$, is computed corresponding to Orlandi and Fatica [8], see Fig. 5.

In order to achieve convergence with the GWJ-EARSM for $Ro = 1$, the 3D mean flow correction proposed by Wallin and Johansson [6] (see Appendix A) was applied. To enable comparisons, the N-correction was also applied to the WJ-EARSM for this rotation number. For $Ro = 0.5$ the cubic N or N^*-solutions were used.

4.1. Mean velocities

The mean axial velocity normalized with the mean bulk velocity, U_z/U_m, is shown in Fig. 1. For $Ro = 0$, all models predict a U_z profile that is somewhat too flat as compared to the experimental data in the region $0 \leqslant r/R \leqslant 0.8$. Hence, the mean velocity becomes underpredicted in the centre of the pipe and too large closer to the wall. The predictions of the two EARSMs collapse to the same curve. The two DRSM formulations differ slightly despite the fact that the total contribution of $\mathbf{N}^{\Omega}$ and $\mathbf{N}^{S}$ is zero. This is due to the recalibration of the model coefficient A_0 for the GWJ-EARSM (something that is inherited by the NL-DRSM and hence affects the predictions), which is necessary to capture neutral stability of a rotating homogenous shear flow for rotation number $Ro = 0.5$, see Grundestam et al. [13] and Wallin and Johansson [19].

Also for $Ro = 0.5$ all models predict a mean axial velocity which is too low in the middle of the pipe. The GWJ-EARSM shows, however, the best agreement with the experimental data and gives a small improvement over the other models. For the WJ-EARSM the change from the $Ro = 0$ case is small, and the two DRSMs predict virtually the same U_z. All models predict a small increase of the centerline velocity as compared with the nonrotating case, in accordance with the experiments.

The predicted increase in centerline velocity from $Ro = 0.5$ to $Ro = 1$ is even larger than in the experiments. For $Ro = 1$, the NL-DRSM agrees well with the experiments. The L-DRSM and the WJ-EARSM predict a U_z-profile that is somewhat too flat in the center of the pipe. The GWJ-EARSM, on the other hand, slightly overshoots in the center of the pipe meaning that the profile is somewhat too laminar-like. Note, though, that for this rotation convergence of the solution required the 3D mean flow corrected approximation for N. This is consistent with the fact that the 3D character of the flow is stronger in this case ($Ro = 1$).

All models predict a near parabolic shape of the mean azimuthal velocity, U_θ, for both $Ro = 0.5$ and $Ro = 1$, see Fig. 2. It is clear that the nonlinear terms $\mathbf{N}^{\Omega}$ and $\mathbf{N}^{S}$, affect the model predictions significantly, resulting in profiles that deviate less from solid body rotation. This implies a better agreement between the nonlinear models and the experiment for $Ro = 0.5$. For $Ro = 1$, on the other hand, the NL-DRSM and the GWJ-EARSM predict a U_θ profile that deviates too little from a solid body rotation. What also can be noted here is that in the experiments by Imao et al. [9], the difference in U_θ/U_w between $Ro = 0.5$ and $Ro = 1$ is small with a small increase in the deviation from solid body rotation for increasing rotation. The model predictions show the opposite trend with a decreasing deviation from solid body rotation for increasing rotation. The trend of decreasing deviation from solid body rotation can also be extracted from the data in the paper by Orlandi and Fatica [8].

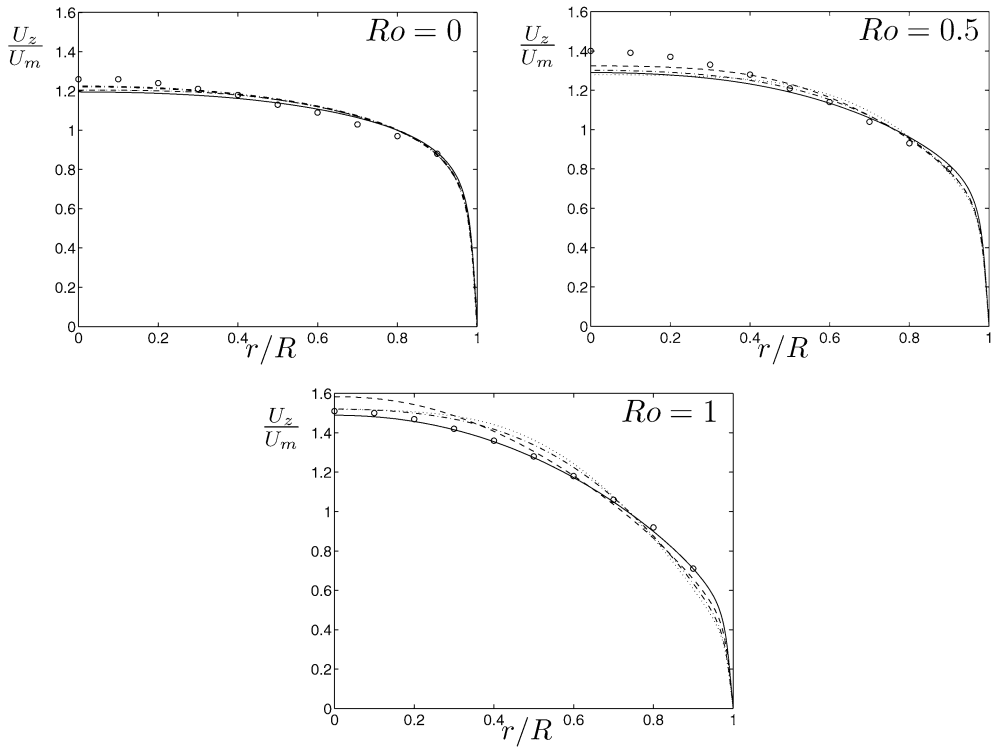

Fig. 1. Normalized axial velocity U_z/U_m for $Re_m = U_m D/\nu = 20\,000$ and $Ro = U_\theta(R)/U_m = 0$, 0.5 and 1, (−) NL-DRSM, (−−) GWJ-EARSM, (−·) L-DRSM (thick line for $Ro = 0$), (···) WJ-EARSM, experimental data by Imao et al. [9] (∘).

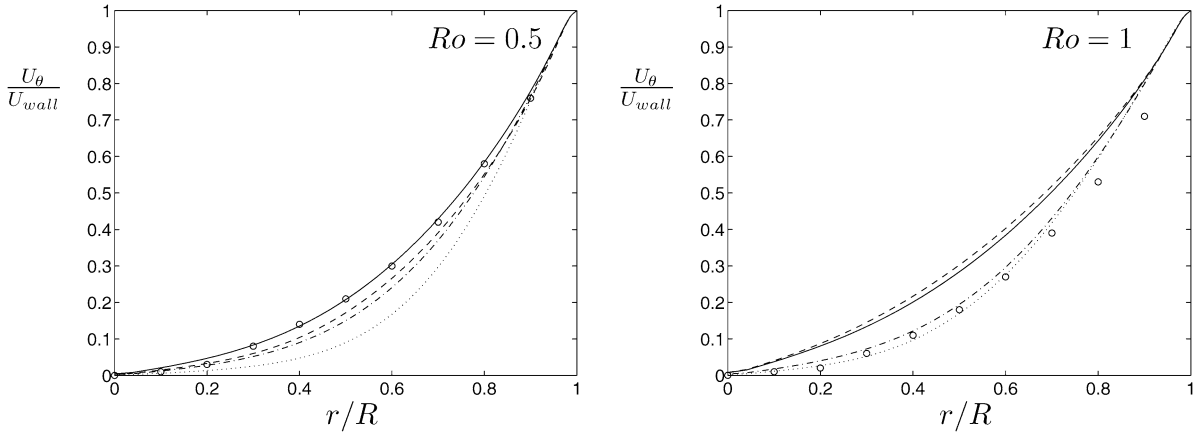

Fig. 2. Normalized azimuthal velocity U_θ/U_{wall} for $Re_m = U_m D/\nu = 20\,000$ and $Ro = U_\theta(R)/U_m = 0.5$ and 1, (−) NL-DRSM, (−−) GWJ-EARSM, (−·) L-DRSM, (···) WJ-EARSM, experimental data by Imao et al. [9] (∘).

4.2. Turbulence kinetic energy

For the nonrotating case (Fig. 3), all model predictions of the turbulence kinetic energy more or less coincide and are in reasonably good agreement with experimental data. The somewhat low values of K in the near-wall region are associated with the high-Re form of the ω-equation used. The latter also holds for the rotating cases.

For nonzero *Ro*, the predictions for all models are still in fair agreement with the experimental data. For $Ro = 0.5$ all models predict a higher level of K in the central region, than for the nonrotating case. The experiments, on the other hand, show a small

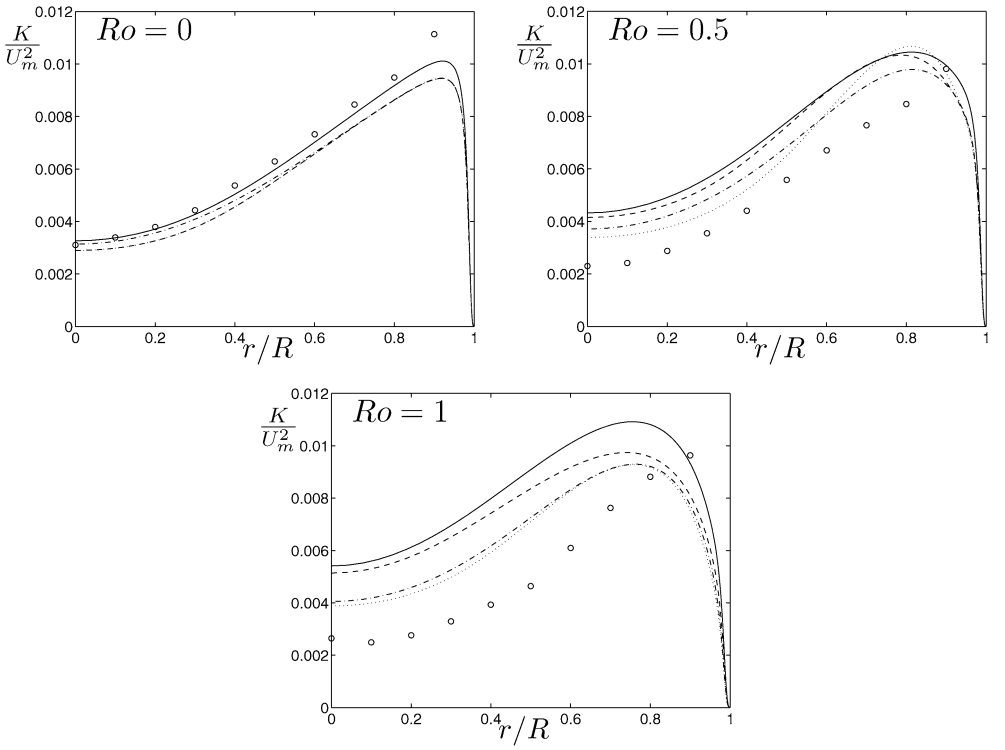

Fig. 3. Normalized turbulence kinetic energy K/U_m^2 for $Re_m = U_m D/\nu = 20\,000$ and $Ro = U_\theta(R)/U_m = 0$, 0.5 and 1, (−) NL-DRSM, (−−) GWJ-EARSM, (−·) L-DRSM, (···) WJ-EARSM, experimental data by Imao et al. [9] (○).

decrease. The NL-DRSM and the GWJ-EARSM show a further increase for $Ro = 1$, while the experimental data show little difference between $Ro = 0.5$ and $Ro = 1$.

4.3. Reynolds stress anisotropies

The effect of the turbulence on the mean flow is directly related to the Reynolds stresses $\overline{u_r u_z}$ and $\overline{u_r u_\theta}$, as seen in (2) and (1). The shape of the U_z-profile is governed by the predicted $\overline{u_r u_z}$ and the deviation from solid body rotation of the azimuthal mean velocity component, U_θ, seen in Fig. 2, is an effect of a nonzero and positive $\overline{u_r u_\theta}$. The model predictions of the diagonal Reynolds stress anisotropies, $a_{\alpha\alpha}$ (repeated α means no summation) influence the mean flow velocity components only in an indirect manner.

The diagonal components, $a_{\alpha\alpha}$, and the off-diagonal components a_{rz} and $a_{\theta z}$ are shown in Fig. 4. Comparisons are made with the experimental data by [9]. Since the experiments do not provide measurements of $\overline{u_r u_\theta}$ the corresponding model predicted anisotropy, $a_{r\theta}$, is compared with the direct numerical simulations by Orlandi and Fatica [8]. Therefore, complementing computations were performed for $Re = 4900$. The model predictions of $a_{r\theta}$ together with the corresponding values of K are shown in Fig. 5. In order to keep the plot as clear as possible, only the predictions made by the DRSM turbulence models are shown here, the L-DRSM and the NL-DRSM. Thus, the effect of the nonlinear terms on the Reynolds stress anisotropies can be studied. The anisotropy predicted by using EARSM and DRSM are qualitatively similar. The most important difference is that the EARSM predicts diagonal Reynolds stress anisotropy components which are nearly zero in the center of the pipe. This is due to the neglected diffusion of the Reynolds stress anisotropy which leads to a direct dependence of a_{ij} on the mean velocity gradients for the EARSM. In the center of the pipe, where $\partial U_z/\partial r$ is zero and $\partial U_\theta/\partial r$ is relatively small and attains its smallest value, the EARSM predictions are nearly isotropic. The DRSMs, on the other hand, do not suffer from this limitation and therefore allow a more physically correct anisotropic turbulence, and hence nonzero $a_{\alpha\alpha}$, in this region.

As seen in Fig. 4 the model predictions of $a_{\alpha\alpha}$ show the same trends as the experiments, with the largest part of the turbulence kinetic energy in the $\overline{u_z u_z}$ component. The quantitative agreement is somewhat better for $Ro = 0.5$ than for $Ro = 1$. The failure of the models close to the wall is a result of the near wall treatment and the fact that no near wall damping has been applied.

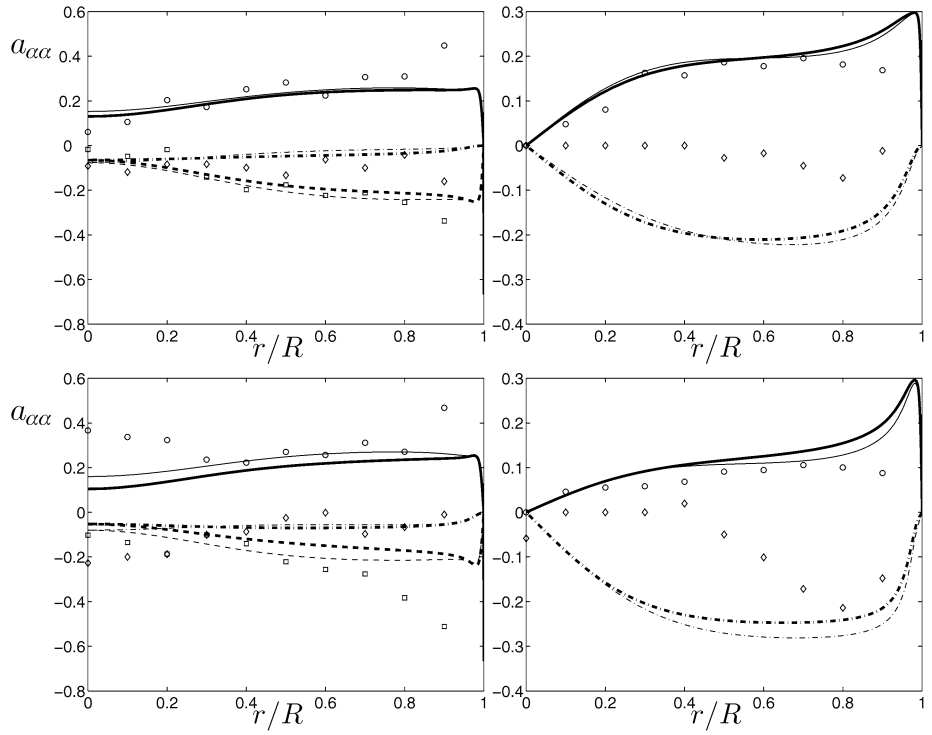

Fig. 4. Reynolds stress anisotropy, a_{ij} for $Ro = 0.5$ (top) and $Ro = 1$ (bottom). Left: a_{zz} $(-)$ and $\circ$, $a_{\theta\theta}$ $(-\cdot)$ and $(\diamond)$ and a_{rr} $(--)$ and $(\square)$. Right: a_{rz} $(-)$ and $(\circ)$ and $a_{\theta z}$ $(-\cdot)$ and $(\diamond)$. L-DRSM (thin line), NL-DRSM (thick line), experimental data by Imao et al. [9] (symbols).

This is also evident for a_{rz}, which is in good agreement with the experiments in the center region while being overpredicted close to the wall. It should further be pointed out that due to the overall decrease of a_{rz} in combination with the relatively small increase of the turbulence kinetic energy when the rotation is increased from $Ro = 0.5$ to $Ro = 1$, $\overline{u_r u_z}$ decreases which results in a more laminar like U_z-profile.

The magnitude of $a_{\theta z}$ is drastically overpredicted. We can further note that both the L-DRSM and the NL-DRSM predict a negative $a_{\theta z}$. The experimental data by Imao et al. [9] also show this. The negative sign of $a_{\theta z}$ is also reported on by for instance Pettersson and Andersson [4] and Jakirlić and Hanjalić [1] when using RANS models to compute rotating pipe flow. Negative $a_{\theta z}$ is in contradiction with the direct numerical simulation by Orlandi and Fatica [8], which has shown a positive $a_{\theta z}$. For further discussions on the $a_{\theta z}$-anomaly, see for instance Petterson and Andersson [4] and Jakirlić and Hanjalić [1].

When comparisons are made with the direct numerical simulations by Orlandi and Fatica [8], see Fig. 5, the nonlinear terms (12) and (13) are seen to clearly have a positive effect on the predictions of $a_{r\theta}$ and the turbulence level K. However, at this Reynolds number the disadvantage of the lack of near wall treatment is obvious. The underprediction of the turbulence kinetic energy close to the wall results in a drastically overpredicted $a_{r\theta}$ in the same region. One can further make the note that in the DNS by Orlandi and Fatica [8], the turbulence kinetic energy levels rather seem to increase with increasing rotation instead of decrease as indicated by the experiments by for instance Imao et al. [9] and Facciolo [10].

The magnitude of $a_{r\theta}$ is much smaller than the other anisotropy components. This is in line with the discussion in Wallin and Johansson [6] that $a_{r\theta}$ should scale as $1/Re$.

4.4. Alternative diffusion modelling for the EARSMs

In the paper by Wallin and Johansson [6], an effective eddy-viscosity diffusion model for the K- and ω-equations was tested in conjunction with their EARSM formulation. The effective eddy-viscosity, ν_T^{eff}, can be seen as the part of Reynolds stress anisotropy that is proportional to the strain rate tensor, S_{ij}, and is given by

$$\nu_T^{\text{eff}} = -\frac{1}{2}(\beta_1 + II_{\Omega^*}\beta_6)K\tau. \tag{21}$$

The resulting diffusion terms of the K and ω equations read

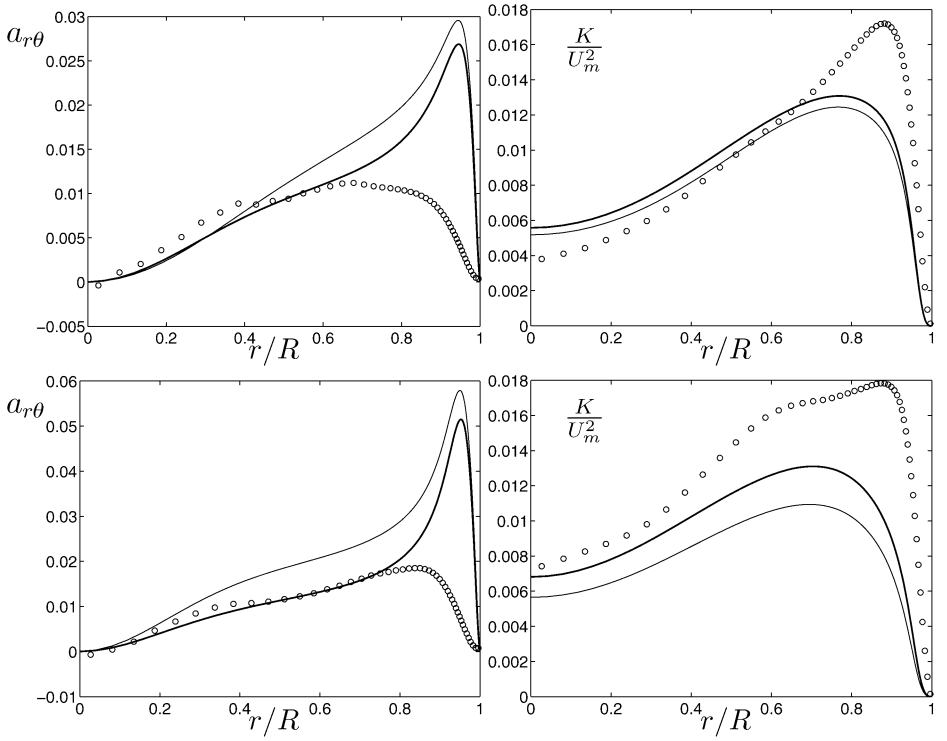

Fig. 5. Computed $a_{r\theta}$ and K/U_m^2 at $Re = 4900$ for $Ro = 0.5$ (upper) and $Ro = 1$ (lower). Left: $a_{r\theta}$, right: K. L-DRSM (thin line), NL-DRSM (thick line), DNS by Orlandi and Fatica [8] (symbols).

$$\mathcal{D}_K = \frac{1}{r}\frac{\partial}{\partial r}\left(r\left(\nu + \frac{\nu_T^{\text{eff}}}{\sigma_K}\right)\frac{\partial K}{\partial r}\right), \tag{22}$$

$$\mathcal{D}_\omega = \frac{1}{r}\frac{\partial}{\partial r}\left(r\left(\nu + \frac{\nu_T^{\text{eff}}}{\sigma_\omega}\right)\frac{\partial \omega}{\partial r}\right) \tag{23}$$

where $\sigma_K = 2$ and $\sigma_\omega = 2$ are model parameters. Compared to a Daly–Harlow model, this model gives only small differences in the predictions of plane turbulent channel flow.

In the present case, however, the use of this modelling approach instead of the Daly and Harlow model, leads to substantial changes in the EARSM predictions. Especially, the predicted values of the turbulence kinetic energy levels become dramatically higher for the rotating cases. This can be seen in Fig. 6, where predictions emanating from the application of the eddy-viscosity diffusion model and the model proposed by Daly and Harlow [17] are compared for $Ro = 0.5$.

From this it is obvious that the application of the effective eddy-viscosity based diffusion model leads to a severe overprediction of the turbulence kinetic energy. Also, the maximum of K is moved closer to the center of the pipe. The eddy viscosity approach in conjunction with the GWJ-EARSM leads to a drastic change of the shape of the K-profile. The level is severely overpredicted and the region where the profile is concave downwards occupies the major part of the pipe. The WJ-EARSM also overpredicts the turbulence level. The region where the second derivative of K is positive and negative, respectively, are not changed nearly as much as for the GWJ-EARSM though. For $Ro = 1$ (not shown here), both models overpredict the turbulence level even more severely showing a maximum peak of $K/U_m^2 \sim 0.03$.

The mechanism behind the high turbulence kinetic energy levels predicted by the eddy-viscosity based diffusion model is further discussed in section 6. Also, it is demonstrated that reasonable turbulence level can be achieved with this diffusion model by slightly altering the model for the production of the dissipation rate in the ω-equation.

4.5. Comparisons with scaling laws from symmetry methods

Lie group symmetry methods are useful tools for analyzing differential equations. The idea is to derive transformations of the independent and dependent variables that leave the form of the governing equations unaltered. These transformations are then said to be symmetries or symmetry transformations of the system considered. By use of these transformations one can reduce

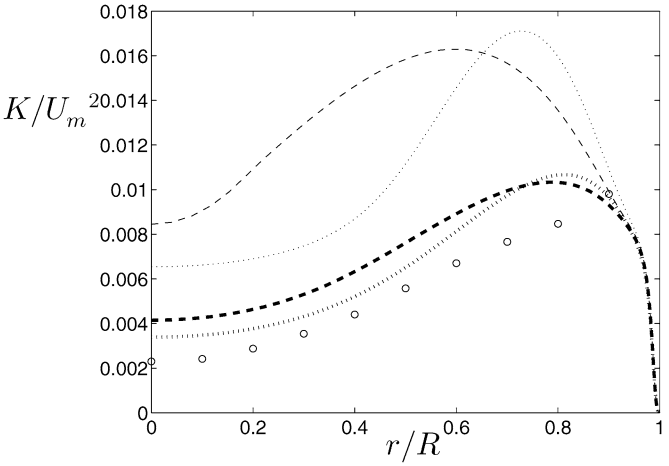

Fig. 6. Computed turbulence kinetic energy, K/U_m^2 for $Ro = 0.5$: WJ-EARSM ($\cdots$) and GWJ-EARSM ($--$); eddy-viscosity based diffusion model (thin) Daly–Harlow diffusion model (thick), experimental data by Imao et al. [9] ($\circ$).

the number of independent variables, and also, compute the relations between the independent and the dependent variables or invariant solutions. The relations are not unique however, but depend on a number of free functions which can be chosen somewhat arbitrarily. By imposing a constraint on a free function, a symmetry is broken. Loosely speaking, this corresponds to imposing outer constraints on the governing system (or boundary conditions) and will lead to a change of the invariant solutions governed by the corresponding free function.

Lie group symmetry methods have been applied to the Navier Stokes equations by e.g. Oberlack [11] for the study of solutions to plane parallel shear flows (and further tested by Lindgren et al. [22]). Oberlack [23] also applied the method to nonrotating and rotating turbulent pipe flows. Similar studies for free shear-flows etc. can be found in Cantwell [24]. For the rotating pipe flow Oberlack derived algebraic scaling laws for the mean axial and azimuthal velocities. The algebraic law for the azimuthal velocity can be written

$$\frac{U_\theta(r)}{U_\theta(R)} = \zeta\left(\frac{r}{R}\right)^{\psi} \tag{24}$$

where $U_\theta(R)$ is the azimuthal velocity at the wall and ζ and ψ are constants. It is assumed to hold away from the pipe wall with $\psi = 2$ and ζ close to unity. The axial mean velocity is strongly dependent on the azimuthal wall velocity, $U_\theta(R)$, therefore Oberlack proposes a velocity defect law for the axial mean velocity

$$\frac{U_c - U_z}{U_\tau} = \chi\left(\frac{U_\theta(R)}{U_\tau}\right)\left(\frac{r}{R}\right)^{\psi} \tag{25}$$

where U_c is the centerline velocity and χ a function of the velocity ratio. The symmetry analysis indicates that ψ should have the same value for (24) and (25), see Oberlack [23].

The scaling law for the azimuthal velocity, (24), is compared with the present computations in Fig. 7. It is obvious that the dependence of the different models on the radial coordinate is not strictly quadratic, but varies. Close to the center of the pipe ($r/R \lesssim 0.3$) all model predictions correspond to $\psi \sim 1$ and $\zeta < 1$. The linear dependence of the azimuthal mean velocity on the radial coordinate near the center of the pipe is also noted by Oberlack [11] when making comparisons with the DNS data by Orlandi and Fatica [8]. For $Re_m = 4900$ and $Ro = 2$, he deduces that the quadratic algebraic law (24) is only valid in the region $0.3 \leqslant r/R \leqslant 0.6$.

At around $r/R \sim 0.3$–0.4, the model predictions of ψ successively increase. For $Ro = 0.5$, the NL-DRSM is in best agreement with (24) and shows for $r/R > 0.3$ a nearly quadratic radial dependence. For $Ro = 1$, on the other hand, the power in the dependence on r for the same model is too low.

Model comparisons with the axial velocity defect law (25) can be seen in Fig. 8. The DRSMs are in good agreement with (25) throughout most of the region and the deviation from the quadratic scaling law seems to be significant for $r/R \geqslant 0.6$ for the linear DRSM and somewhat closer to the wall for the NL-DRSM. For $Ro = 0.5$, the EARSMs has varying dependence on the radial coordinate corresponding to $\psi \sim 1.5$–3. This is also the case for the WJ-EARSM for $Ro = 1$.

The experimental data by Imao are plotted in Figs. 7 and 8 for comparison and are generally in good agreement with the quadratic scaling laws (24) and (25), respectively. Smaller deviations can be seen for U_θ, Fig. 7, in the region $r/R \leqslant 0.3$, especially for $Ro = 1$.

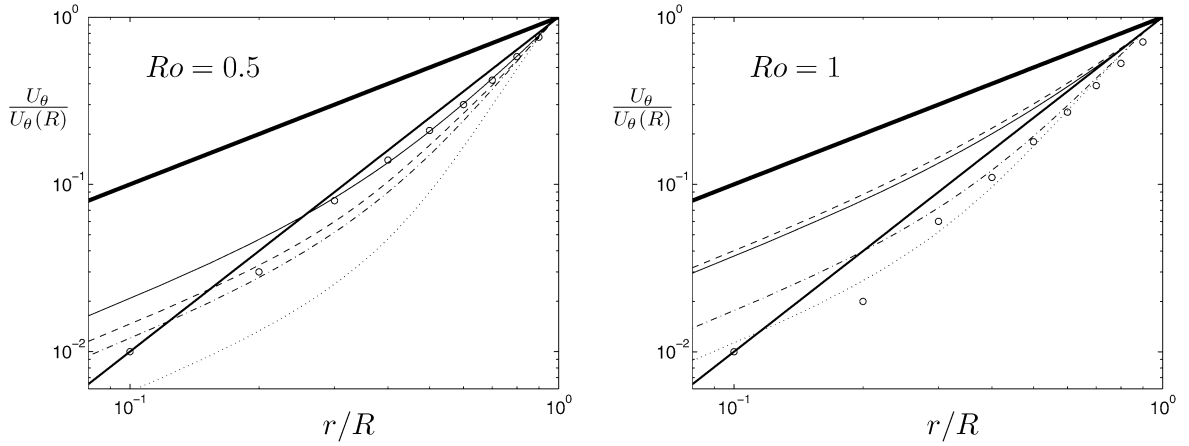

Fig. 7. Log–log-plot of normalized azimuthal velocity $U_\theta/U_\theta(R)$ for $Re_m = U_m D/\nu = 20\,000$ and $Ro = 0.5$ and 1. (−) NL-DRSM, (−−) GWJ-EARSM, (−·) L-DRSM, (···) WJ-EARSM, experimental data by Imao et al. [9] (○), straight lines $\sim (r/R)$ (thickest) and $\sim (r/R)^2$ (thick).

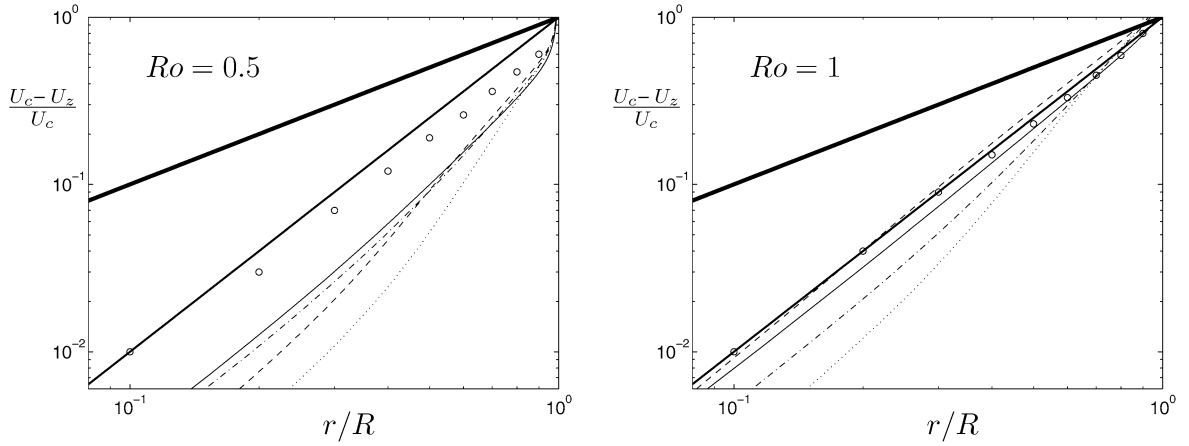

Fig. 8. Log–log-plot of normalized velocity defect for $Re_m = U_m D/\nu = 20\,000$ and $Ro = 0.5$ and 1. (−) NL-DRSM, (−−) GWJ-EARSM, (−·) L-DRSM, (···) WJ-EARSM, experimental data by Imao et al. [9] (○), straight lines $\sim (r/R)$ (thickest) and $\sim (r/R)^2$ (thick).

5. Approximation of N and neglection of diffusion of the Reynolds stress anisotropy in EARSM

Although both the EARSMs and the DRSMs give qualitatively good predictions for this particular flow case, it may be interesting to investigate how the differences between the models affect the predictions.

The important differences between the EARSMs and the DRSMs used in the present study, are the approximation of the quantity $\mathcal{P}/\varepsilon$ used in the expansion coefficients of the EARSM and the neglection of the diffusion of the Reynolds stress anisotropy due to the EARSM weak equilibrium assumption. In order to eliminate as many differences between the EARSM and DRSM as possible, only the WJ-EARSM and the L-DRSM will be investigated here. Although, the NL-DRSM and GWJ-EARSM are closely related, the approximations of the nonlinear terms $\mathbf{N}^{\Omega}$ and $\mathbf{N}^{S}$ in the GWJ-EARSM, introduce differences in addition to those mentioned above.

To get a more quantitative indication on how the $\mathcal{P}/\varepsilon$-approximation and the neglection of the diffusion of the Reynolds stress anisotropy affect the predictions of the production to dissipation ratio, $\mathcal{P}/\varepsilon = -\tau\{\mathbf{aS}\}$, in the transport equation of K, one can by using the K, ω and mean flow solutions from the L-DRSM, calculate $\mathcal{P}/\varepsilon = -\tau\{\mathbf{aS}\}$ as given by the WJ-EARSM under the conditions: (a) N in the β-coefficients is calculated using $\mathcal{P}/\varepsilon$ from the L-DRSM solution; (b) N is calculated using the solution of the cubic equation as an approximation; (c) N is calculated using the cubic equation plus the 3D mean flow correction (see Appendix A).

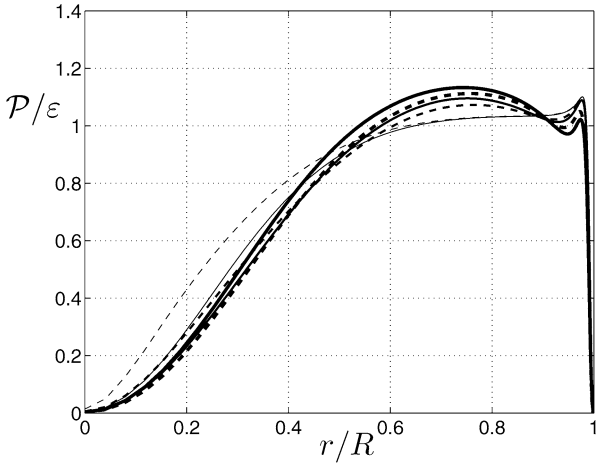

Fig. 9. $\mathcal{P}/\varepsilon = -\tau\{\mathbf{aS}\}$ for $Ro = 0$ (thin line), 0.5 (thicker line) and 1 (thickest line) for L-DRSM (−). (−−) $\mathcal{P}/\varepsilon$ as predicted by the WJ-EARSM using N from the L-DRSM flow solution.

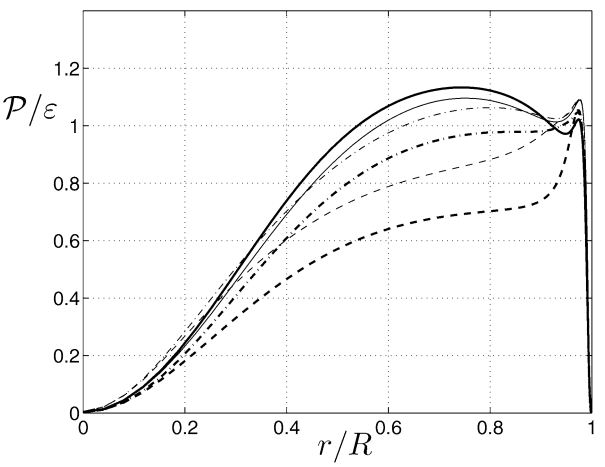

Fig. 10. $\mathcal{P}/\varepsilon = -\tau\{\mathbf{aS}\}$ for $Ro = 0.5$ (thin line), and 1 (thick line) for L-DRSM (−), WJ-EARSM (−−) and WJ-EARSM with N-correction (−·) using the L-DRSM mean flow, K and ω solutions.

The outcome can be interpreted by looking at the balance equation of the Reynolds stress anisotropy for the fully developed flow, which is satisfied by the DRSM solution,

$$\frac{1}{\varepsilon}\left(\frac{\overline{u_i u}_j}{K}\mathcal{D}_K - \mathcal{D}_{ij}\right) = -\frac{K}{\varepsilon}\mathcal{A}_{ij} + \frac{1}{\varepsilon}(\mathcal{P}_{ij} - \varepsilon_{ij} + \Pi_{ij}) - \frac{\overline{u_i u}_j}{K}\left(\frac{\mathcal{P}}{\varepsilon} - 1\right) \tag{26}$$

where $\mathcal{A}_{ij}$ is the advection of a_{ij} which is fully accounted for in the EARSM calculations, see Section 2.1. The left-hand side of (26) is the total diffusion of a_{ij} which is neglected for the EARSM meaning that only the right-hand side of (26) is zero when $\mathcal{P}/\varepsilon$ from the explicit algebraic model is inserted.

For case (a), the difference between the EARSM and DRSM indicates to what extent the neglection of the diffusion of a_{ij} alters the production to dissipation ratio in the transport equation of K. The difference between cases (a) and (b) shows how the cubic approximation of N in the β-coefficients affects the production to dissipation ratio in the transport equation of K.

For case (a), the difference between the DRSM and the EARSM in the predictions of $\mathcal{P}/\varepsilon$ are small, especially for the rotating cases (see Fig. 9). However, by investigating case (b) (Fig. 10) and comparing with case (a), one can deduce that the approximation of N affects the flow predictions significantly more than the neglection of the diffusion of a_{ij} for the rotating cases. In fact, the approximation of N becomes increasingly more important as the rotation is increased. This is consistent with the fact that the cubic N-approximation is exact for 2D mean flows only and can hence be expected to deviate more and more from the exact value as the effects of a 3D mean flow become stronger due to increased rotation. What is important to note here, is that both the neglection of the diffusion and the approximation of N could be expected to have an overall damping effect on the turbulence for the rotating cases according to Figs. 9 and 10.

Case (c) illustrates the significant improvement achieved by use of the 3D mean flow correction for N (see Appendix A). Although the improvement for $Ro = 1$ is relatively smaller than for $Ro = 0.5$ it is important since the effects of the 3D character of the flow become more and more important with increasing rotation. It should also be noted that the GWJ-EARSM requires the 3D N-correction for convergence at $Ro = 1$, see [20].

6. Discussion

It is obvious that the nonlinear terms $\mathbf{N}^{\Omega}$ and $\mathbf{N}^{S}$ have a significant effect on the predictions of axially rotating pipe flow. For the explicit algebraic model formulation this means an overall improvement for $Ro = 0.5$. For the DRSMs the nonlinear terms also have a significant effect on the predictions. But in this case it is not clear whether $\mathbf{N}^{\Omega}$ and $\mathbf{N}^{S}$ have an overall positive effect. It is evident, however, that the effect of $\mathbf{N}^{\Omega}$ and $\mathbf{N}^{S}$ is not as pronounced for the DRSM as for the EARSM.

The differences between the predictions made by the DRSM and the EARSM can be expected to depend on two differences between the two modelling approaches. The first is the consistency condition for the explicit algebraic models. a_{ij} is explicitly dependent on $N = A_3 + A_4\frac{\mathcal{P}}{\varepsilon}$ which should be consistent with the relation $\mathcal{P}/\varepsilon = -\tau\{\mathbf{aS}\}$. This results in a cubic equation for N (or $\mathcal{P}/\varepsilon$) in 2D mean flows which can be solved, see Girimaji [25] and Wallin and Johansson [6]. In 3D mean flows,

N is given by a sixth order equation which cannot readily be solved. Therefore the 2D mean flow form of N is used as an approximation, see Wallin and Johansson [6]. For a DRSM no such approximation is necessary since no explicit dependence of a_{ij} on $\mathcal{P}/\varepsilon$ is needed. The second factor to consider is the diffusion modelling. For the EARSM, the diffusion of the Reynolds stress anisotropy is neglected due to the underlaying weak equilibrium assumption. We here also found that it is important to a choose a Daly–Harlow type of diffusion modelling in the platform (K–ω, here) equations, especially for the prediction of reasonably correct kinetic energy levels.

To understand how the interaction between the production to dissipation ratio and the diffusion terms affects the predictions, one can consider a simplified transport equation of some quantity ϕ for modelling the principal behaviour in e.g. the K-equation

$$\frac{\partial \phi}{\partial t} = \mathcal{P}_\phi - \varepsilon_\phi + \frac{\partial}{\partial x}\left(c_1 \frac{\partial \phi}{\partial x}\right), \quad x \in [0, 1]. \tag{27}$$

For an unsteady state, the local value of $\mathcal{P}_\phi - \varepsilon_\phi$ will correspond to the local rate of change due to the total source term. The diffusion term will locally act as a source or sink depending on whether the second derivative of ϕ is positive or negative, assuming that c_1 is a positive constant.

For a steady state (fully developed) the situation is a bit different since the left-hand side of (27) vanishes. If c_1 is assumed to be a positive constant, then, whether $\mathcal{P}_\phi/\varepsilon_\phi < 1$ or $\mathcal{P}_\phi/\varepsilon_\phi > 1$ determines the sign of the second derivative of ϕ. If the region where $\mathcal{P}_\phi/\varepsilon_\phi > 1$ is wide, the ϕ-profile will be concave downwards over a large region with a local curvature depending on the local value of $\mathcal{P}_\phi/\varepsilon_\phi$ and c_1 in the corresponding region. A small region in conjunction with a small value c_1 would, on the other hand, result in a narrow sharp peak in the ϕ-profile. The situation is the opposite in regions where $\mathcal{P}_\phi/\varepsilon_\phi < 1$ where a small value of c_1 gives a profile which is strongly concave upwards. Intuitively this is correct since a large diffusion, large value of c_1, tends to smear things out and suppress peaks. The requirement of $\mathcal{P}_\phi/\varepsilon_\phi > 1$ in some region also poses a condition on the existence of a nonzero solution. If the boundary conditions are given by $\partial\phi/\partial x = 0$ and $\phi = 0$ in the center and on the wall of the pipe respectively, as in the present computations, and only $\phi \geqslant 0$ is allowed, then it is a necessity to have $P_\phi/\varepsilon_\phi > 1$ somewhere in the domain in order to obtain a nonzero solution. The reason for this is that if $\mathcal{P}_\phi/\varepsilon_\phi \leqslant 1$ everywhere, which implies a positive second derivative, then ϕ must be zero or negative in the domain to match the boundary conditions. Since negative values are not allowed, for e.g. $\phi = K$, the zero solution will be the only solution.

For the actual computations, the diffusion cannot be formulated in terms of a pure second derivative of K as in (27) since the diffusion model gives rise to extra terms that have to be taken into account (c_1 is not constant). This implies for example that the point where the second derivative of K changes sign is not located at the same point as where $\mathcal{P}/\varepsilon = 1$. However, $\mathcal{P}/\varepsilon = 1$ will correspond to the point where the diffusion of K changes sign and will hence give an indication on where $\nabla_r^2 K$ changes sign. It is also evident that the diffusion modelling plays a significant role. This is demonstrated in Section 4.4 where the application of the eddy-viscosity based diffusion model leads to severe overpredictions of K for the rotating cases. One can also, by adjusting c_s and c_ω, alter the turbulence level. In fact, it can readily be demonstrated that an increase in c_s results in lower K-values close to the wall and increased turbulence levels in the center of the pipe. A decrease has the opposite effect. This is consistent with the fact that turbulence is mainly produced in the near-wall region and transported outwards. For the ω-equation, on the other hand, an increase in c_ω results in an overall decrease in K while a decrease has the opposite effect for this particular case.

However, one must remember that the model predictions of the turbulence kinetic energy are governed by a very fine balance which is strongly related to the lengthscale determining equation. In particular, the modelling of the production of the lengthscale determining quantity, $\mathcal{P}_\omega$ in our case, is very important since K is strongly influenced via the prediction of ω. It can be shown that a small change in P_ω can have a significant effect on the turbulence levels. As a demonstration of this one can use the eddy-viscosity based effective diffusion model discussed above in conjunction with a modified model for $\mathcal{P}_\omega$. By blending the eddy-viscosity assumption with an EARSM when computing $\mathcal{P}_\varepsilon$, a model for the production of the dissipation rate can be obtained, $\mathcal{P}_\varepsilon = C_{\varepsilon 1}\varepsilon/K(C_\alpha \mathcal{P}_K^{\mathrm{EVM}} + (1 - C_\alpha)\mathcal{P}_K^{\mathrm{EARSM}})$ where $\mathcal{P}_K^{\mathrm{EVM}} = 2\nu_T II_S$ and C_α is the parameter that determines the relative weight of the eddy viscosity assumption. Since the production of ω is given by $\mathcal{P}_\omega = \mathcal{P}_\varepsilon/(C_\mu K) - \frac{\omega}{K}\mathcal{P}_K$, $\mathcal{P}_\omega$ becomes

$$\mathcal{P}_\omega = 2C_\alpha(\alpha + 1)II_S + (\alpha - C_\alpha - C_\alpha\alpha)\frac{\omega}{K}\mathcal{P}_K \tag{28}$$

where $\alpha = C_{\varepsilon 1} - 1$ and $\mathcal{P}_K$ denotes the turbulent kinetic energy production.

By using (28) in the K–ω platform the characteristics of the flow are radically changed even for a small value of C_α. Fig. 11 shows the predictions made by the GWJ-EARSM for $C_\alpha = 0.1$ and $C_\alpha = 0$ and $Ro = 0.5$ with the eddy-viscosity based diffusion. As can be seen, the effect on the turbulence kinetic energy is significant and the predictions for $C_\alpha = 0.1$ are in good agreement with the experiments. The mean velocities are not shown here, but the effect on the U_z- and U_θ-profiles is small compared to the change of K. By increasing C_α further the turbulence level is reduced even more while still keeping the change in the mean velocity profiles relatively small.

It must be pointed out, however, that it is not the intention here to investigate the advantages and disadvantages of (28) as a model. Remember that the Daly and Harlow diffusion model gave a much better prediction of K for $C_\alpha = 0$. The purpose is

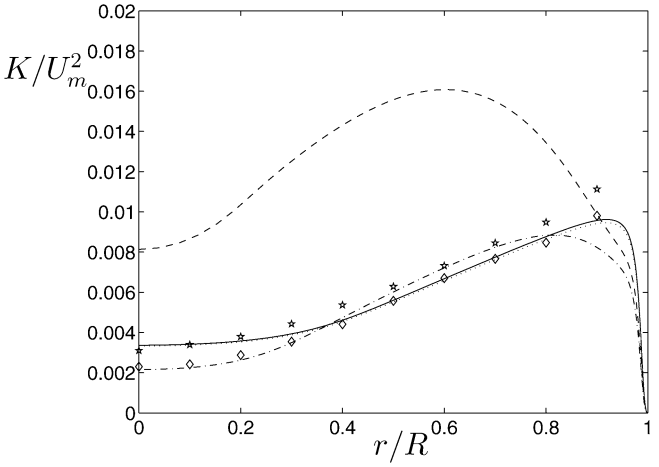

Fig. 11. $\mathcal{P}/\varepsilon$ for GWJ-EARSM and $Ro = 0$ with $C_\alpha = 0$ $(-)$ and $C_\alpha = 0.1$ $(\cdots)$ and for $Ro = 0.5$ with $C_\alpha = 0$ $(--)$ and $C_\alpha = 0.1$ $(-\cdot)$. Diffusion of K and ω based on the effective eddy-viscosity. Experimental data by Imao et al. [9] for $Ro = 0$ $(\star)$, and $Ro = 0.5$ $(\diamond)$.

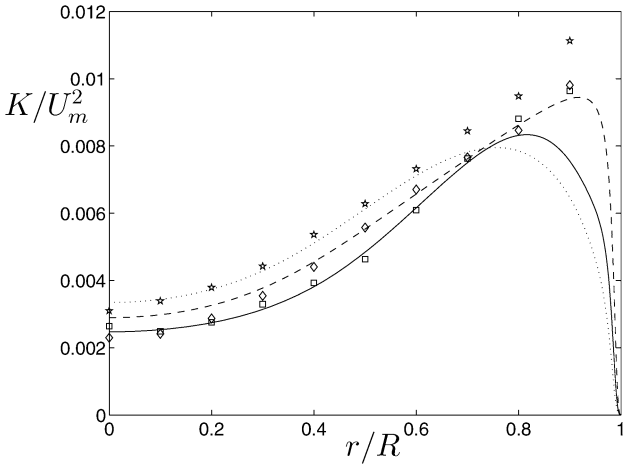

Fig. 12. Normalized turbulence kinetic energy, K/U_m^2, WJ-EARSM with turbulence kinetic energy production, $\mathcal{P}$, calculated from cubic N-equation, for $Ro = 0$ $(--)$, $Ro = 0.5$ $(-)$ and $Ro = 1$ with N-correction $(\cdots)$. Experimental data by Imao et al. [9] for $Ro = 0$ $(\star)$, $Ro = 0.5$ $(\diamond)$ and $Ro = 1$ $(\square)$.

merely to demonstrate that the modelling of $\mathcal{P}_\omega$ is important and that the delicate nature of the problem implies that a small change in the model can have a significant effect on the turbulence level.

In the present EARSM computations the approximation of $\mathcal{P}/\varepsilon$ is only used for the β-coefficients, see Appendix A. In the platform equations the production of the turbulence kinetic energy is naturally calculated as $\mathcal{P} = -K\{\mathbf{aS}\}$, with S_{ij} given by (4). In this way the production of the turbulence kinetic energy, $\mathcal{P}$, is consistent with the formulation of the Reynolds stress anisotropy in the sense that $\mathcal{P}$ is exact in terms of a_{ij}. The alternative to this would be to make $\mathcal{P}$ consistent with N and hence evaluate the production of the turbulence kinetic energy as $\mathcal{P} = (N - A_3)\varepsilon/A_4$. For the WJ-EARSM this leads to turbulence kinetic energies in good agreement with the experiments, see Fig. 12. For $Ro = 0.5$ this approach leads to a small decrease in K compared to the nonrotating case. If the N-correction is applied for $Ro = 1$ the predictions of K are in reasonable agreement with the experimental data as seen in Fig. 12, slightly better than the previous choice shown in Fig. 3. On the other hand if the N-correction is not applied, the WJ-EARSM predicts a laminar flow for $Ro = 1$, implying stronger sensitivity to flow laminarization. This is another illustration of the importance of the consistency between the production term and N.

Acknowledgement

This work has been carried out within the HiAer project (High Level Modelling of High Lift Aerodynamics). The HiAer project is a collaboration between DLR, ONERA, KTH, HUT, TUB, Alenia, Airbus-D, QinetiQ and FOI. The project is managed by FOI and is partly funded by the European Union (Project Ref: G4RD-CT-2001-00448).

Appendix A. Explicit algebraic Reynolds stress model formulation

In the following the strain and rotation rate tensors are assumed to have been nondimensionalized with the turbulence time scale, τ. The EARSM formulations are derived by solving the modelled ARSM equation which for the GWJ-EARSM reads

$$N\mathbf{a} = -A_1\mathbf{S} - (\mathbf{a}\boldsymbol{\Omega}^* - \boldsymbol{\Omega}^*\mathbf{a}) + c\big(\mathbf{N}^{\Omega} + \mathbf{N}^{S}\big) \tag{A.1}$$

where

$$N = A_3 + A_4\frac{\mathcal{P}}{\varepsilon} \tag{A.2}$$

(A.1) is given by (3) after assuming weak equilibrium, Rodi [18]. Due to the amount of algebra generated, the nonlinear terms, $\mathbf{N}^{\Omega,S}$, are approximated as

$$\mathbf{N}^{\Omega} = \frac{\sqrt{-II_{\Omega}}}{-II_{\Omega^*}}\left(\mathbf{a}\boldsymbol{\Omega}^{*2} + \boldsymbol{\Omega}^{*2}\mathbf{a} - \frac{2}{3}\big\{\mathbf{a}\boldsymbol{\Omega}^{*2}\big\}\mathbf{I}\right), \qquad \mathbf{N}^{S} = \sqrt{II_S}\,\mathbf{a} \tag{A.3}$$

when (A.1) is solved. The approximations reduce to the original expression in 2D mean flows, see Grundestam et al. [13] for further details.

The explicit algebraic models used are formulated using a complete five element tensor basis for 3D mean flows. The basis tensors used are

$$\begin{aligned}
&\mathbf{T}^{(1)} = \mathbf{S}, \quad \mathbf{T}^{(3)} = \boldsymbol{\Omega}^{*2} - \frac{1}{3}II_{\Omega^*}\mathbf{I},\\
&\mathbf{T}^{(4)} = \mathbf{S}\boldsymbol{\Omega}^* - \boldsymbol{\Omega}^*\mathbf{S}, \quad \mathbf{T}^{(6)} = \mathbf{S}\boldsymbol{\Omega}^{*2} + \boldsymbol{\Omega}^{*2}\mathbf{S} - \frac{2}{3}IV\mathbf{I},\\
&\mathbf{T}^{(9)} = \boldsymbol{\Omega}^*\mathbf{S}\boldsymbol{\Omega}^{*2} - \boldsymbol{\Omega}^{*2}\mathbf{S}\boldsymbol{\Omega}^*
\end{aligned}$$

where $\mathbf{S}$ and $\boldsymbol{\Omega}^*$ in this appendix have been normalized using the turbulence timescale

$$\tau = \frac{K}{\varepsilon}. \tag{A.4}$$

The relation between the Reynolds stress anisotropy and the mean flow gradients is given by

$$\mathbf{a} = \beta_1\mathbf{T}^{(1)} + \beta_3\mathbf{T}^{(3)} + \beta_4\mathbf{T}^{(4)} + \beta_6\mathbf{T}^{(6)} + \beta_9\mathbf{T}^{(9)} \tag{A.5}$$

where the β-coefficients are given by

$$\begin{aligned}
\beta_1 &= A_1\big(N^*c^2II_{\Omega} + 8cII_{\Omega^*}\sqrt{-II_{\Omega}} - 14N^*II_{\Omega^*} + 4N^{*3}\big)\big/(Q_1Q_2),\\
\beta_3 &= 4IVA_1\big(2c^2II_{\Omega}N^{*2} + c^3N^*(-II_{\Omega})^{3/2} - 18II_{\Omega^*}^2 + 18cN^*\sqrt{-II_{\Omega}}\,II_{\Omega^*}\\
&\quad + 7c^2II_{\Omega^*}II_{\Omega}\big)\big/\big(II_{\Omega^*}^2\big(2c\sqrt{-II_{\Omega}} - 3N^*\big)Q_1Q_2\big),\\
\beta_4 &= 4A_1/Q_1,\\
\beta_6 &= -2A_1\big(N^*c^2II_{\Omega} + 4cII_{\Omega^*}\sqrt{-II_{\Omega}} + 2N^{*2}c\sqrt{-II_{\Omega}} - 6N^*II_{\Omega^*}\big)\big/(II_{\Omega^*}Q_1Q_2),\\
\beta_9 &= 2A_1\big(4cN^*\sqrt{-II_{\Omega}} + c^2II_{\Omega} - 6II_{\Omega^*}\big)\big/(II_{\Omega^*}Q_1Q_2)
\end{aligned} \tag{A.6}$$

where

$$\begin{aligned}
Q_1 &= -\big(2N^* - c\sqrt{-II_{\Omega}}\big)^2 + 2II_{\Omega^*},\\
Q_2 &= N^{*2} - 2II_{\Omega^*},
\end{aligned} \tag{A.7}$$

$$N^* = A_3^* + A_4\frac{\mathcal{P}}{\varepsilon} \tag{A.8}$$

Table A.1
Model parameters for the pressure strain and dissipation rate anisotropy model

	C_1^0	C_1^1	C_2	C_3	C_4	C_Ω
WJ-EARSN, L-DRSM	4.6	1.24	0.47	2	0.56	0
GWJ-EARSM, NL-DRSM	5.24	2.05	0.25	2	0.2	0.5

where

$$N^* = \begin{cases} \dfrac{A_3^*}{3} + \left(P_1 + \sqrt{P_2}\right)^{1/3} + \operatorname{sign}\left(P_1 - \sqrt{P_2}\right)\left|P_1 - \sqrt{P_2}\right|^{1/3} & P_2 \geqslant 0, \\ \dfrac{A_3^*}{3} + 2\left(P_1^2 - P_2\right)^{1/6} \cos\left(\dfrac{1}{3}\arccos\left(\dfrac{P_1}{\sqrt{P_1^2 - P_2}}\right)\right), & P_2 < 0 \end{cases} \tag{A.9}$$

and

$$P_1 = \left(\frac{A_3^{*2}}{27} + \frac{A_1 A_4}{6} II_S - \frac{2}{3} II_{\Omega^*}\right) A_3^*, \tag{A.10}$$

$$P_2 = P_1^2 - \left(\frac{A_3^{*2}}{9} + \frac{A_1 A_4}{3} II_S + \frac{2}{3} II_{\Omega^*}\right)^3, \tag{A.11}$$

$$A_3^* = A_3 - c\left(\sqrt{II_S} - \sqrt{-II_\Omega}\right). \tag{A.12}$$

For the GWJ-EARSM $c = -C_\Omega / A_0$ where $C_\Omega = 0.5$, see [13]. The EARSM by Wallin and Johansson is retrieved by putting $C_\Omega = 0$ and hence $N^* \to N$. For both EARSMs the model parameters are $\{A_1 = 1.2, A_2 = 0, A_3 = 1.8, A_4 = 2.25\}$. Note that $\boldsymbol{\Omega}^*$ denotes the curvature corrected rotation rate tensor $\boldsymbol{\Omega}$ as defined in (20). For the WJ-EARSM $A_0 = -0.72$ and for the GWJ-EARSM $A_0 = -0.9$. Since $A_1 - A_4$ are kept constant and A_0 is recalibrated when the nonlinear pressure strain rate model is used, the model parameters in (11) are changed according to Table A.1.

For 3D mean flows the exact expression for N is given by the solution to a sixth order polynomial equation, for which no analytical solution has been found. Therefore, the corresponding 2D solution, which is given by a cubic equation, is often used as an approximation also for 3D mean flows. Wallin and Johansson [6] used the sixth order equation to derive a correction to the cubic solution for 3D mean flows. The corrected N is on the form

$$N_{\text{corr}} = N^* + \frac{162(\phi_1 + \phi_2 N^{*2})}{D} \tag{A.13}$$

where the denominator, D, is given by

$$D = 20N^{*4}\left(N^* - \frac{1}{2}c_1'\right) - \tau^2 II_{\Omega^*}\left(10N^{*3} + 15c_1' N^{*2}\right) + 10c_1'\tau^2 II_{\Omega^*}^2 \tag{A.14}$$

and

$$\phi_1 = IV^2 \quad \phi_2 = (V - II_S II_{\Omega^*}/2) \tag{A.15}$$

where

$$II_s = \{\mathbf{S}^2\}, \quad II_{\Omega^*} = \{\boldsymbol{\Omega}^{*2}\}, \quad IV = \{\mathbf{S}\boldsymbol{\Omega}^{*2}\}, \quad V = \{\mathbf{S}^2\boldsymbol{\Omega}^{*2}\}. \tag{A.16}$$

Note that for the rotating pipe case IV is zero. V is not zero, however, and for a 2D mean flow $V^{2\text{D}} = \frac{1}{2} II_S^{2\text{D}} II_{\Omega^*}^{2\text{D}}$ ($\phi_2 = 0$). Therefore, N_{corr} can be written $N_{\text{corr}} = N^*(1 + \psi)$ where $\psi = 162\phi_2 N^*/D$. ψ can thus be seen as the relative influence of the correction on N_{corr} compared to N^*. ψ is plotted in Fig. A.1. From this point of view, the 3D character of the mean flow is clearly stronger for $Ro = 1$ than for $Ro = 0.5$. If the N-correction is not used for $Ro = 1$, ψ attains even larger values.

Appendix B. Daly and Harlow diffusion model for cylindrical geometry

In a cylindrical geometry the modelled diffusion described by (14) and (15) can be conveniently split into two parts according to

$$\mathcal{D}_{ij} = \frac{1}{r}\frac{\partial}{\partial r}\left[r\left(\nu + c_s \frac{K}{\varepsilon}\overline{u_r u_r}\right)\frac{\partial \overline{u_i u}_j}{\partial r}\right] + \mathcal{D}_{ij}^{(\text{ex})} \tag{B.1}$$

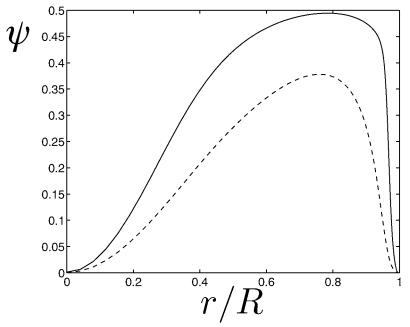

Fig. A.1. ψ from WJ-EARSM for $Ro = 0.5$ (−−) and $Ro = 1$ (−) with N-correction.

$\mathcal{D}_{ij}^{(\mathrm{ex})}$ consists of all the terms that arise due to differentiation of the basis vectors with respect to the azimuthal coordinate, θ. $\mathcal{D}_{ij}^{(\mathrm{ex})}$ is symmetric and traceless and its components read

$$
\begin{aligned}
\mathcal{D}_{r\theta}^{(\mathrm{ex})} &= \frac{1}{r}\frac{\partial}{\partial r}\left[c_s\frac{K}{\varepsilon}\overline{u_r u}_\theta(\overline{u_r u}_\theta - \overline{u_\theta u}_\theta)\right] + c_s\frac{K}{\varepsilon}\frac{\overline{u_r u}_\theta}{r}\left[\frac{\partial}{\partial r}(\overline{u_r u}_r - \overline{u_\theta u}_\theta - 4\frac{\overline{u_\theta u}_\theta}{r})\right] - 4\nu\frac{\overline{u_r u}_\theta}{r^2},\\
\mathcal{D}_{rr}^{(\mathrm{ex})} &= \frac{1}{r}\frac{\partial}{\partial r}\left[-2c_s\frac{K}{\varepsilon}\overline{u_r u}_\theta^2\right] - 2c_s\frac{K}{\varepsilon}\left[\frac{\overline{u_r u}_\theta}{r}\frac{\partial\overline{u_r u}_\theta}{\partial r} + \frac{\overline{u_\theta u}_\theta(\overline{u_r u}_r - \overline{u_\theta u}_\theta)}{r^2}\right] - 2\nu\frac{\overline{u_r u}_r - \overline{u_\theta u}_\theta}{r^2},\\
\mathcal{D}_{\theta\theta}^{(\mathrm{ex})} &= -\mathcal{D}_{rr}^{(\mathrm{ex})},\\
\mathcal{D}_{rz}^{(\mathrm{ex})} &= \frac{1}{r}\frac{\partial}{\partial r}\left[c_s\frac{K}{\varepsilon}\overline{u_r u}_\theta\right]\overline{u_\theta u}_z - c_s\frac{K}{\varepsilon}\left[\frac{\overline{u_\theta u}_\theta}{r^2}\overline{u_r u}_z + 2\frac{\overline{u_r u}_\theta}{r}\frac{\partial\overline{u_\theta u}_z}{\partial r}\right] - \nu\frac{\overline{u_r u}_z}{r^2},\\
\mathcal{D}_{\theta z}^{(\mathrm{ex})} &= \frac{1}{r}\frac{\partial}{\partial r}\left[c_s\frac{K}{\varepsilon}\overline{u_r u}_\theta\right]\overline{u_r u}_z - c_s\frac{K}{\varepsilon}\left[\frac{\overline{u_\theta u}_\theta}{r^2}\overline{u_\theta u}_z - 2\frac{\overline{u_r u}_\theta}{r}\frac{\partial\overline{u_r u}_z}{\partial r}\right] - \nu\frac{\overline{u_\theta u}_z}{r^2},\\
\mathcal{D}_{zz}^{(\mathrm{ex})} &= 0.
\end{aligned}
\tag{B.2}
$$

References

[1] S. Jakirlić, K. Hanjalić, C. Tropea, Modeling rotating and swirling turbulent flows: a perpetual challenge, AIAA J. 40 (2002) 1984–1996.
[2] S. Fu, P.G. Huang, B.E. Launder, M.A. Leschziner, A comparison of algebraic and differential second-moment closures for axisymmetric turbulent shear flows with and without swirl, J. Fluids Engrg. 110 (1988) 216–221.
[3] S. Hirai, T. Takagi, M. Matsumoto, Predictions of the laminarization phenomena in an axially rotating pipe flow, J. Fluids Engrg. 110 (1988) 424–430.
[4] B.A. Pettersson, H.I. Andersson, A.S. Brunvoll, Modeling near-wall effects in axially rotating pipe flow by elliptic relaxation, AIAA J. 36 (1998) 1164–1170.
[5] P.A. Durbin, A Reynolds-stress model for near-wall turbulence, J. Fluid Mech. 249 (1993) 465–498.
[6] S. Wallin, A.V. Johansson, An explicit algebraic Reynolds stress model for incompressible and compressible turbulent flows, J. Fluid Mech. 403 (2000) 89–132.
[7] J.G.M. Eggels, B.J. Boersma, F.T.M. Nieuwstadt, Direct and large-eddy simulations of turbulent flow in an axially rotating pipe, Lab. for Aero- and Hydrodynamics, Delft Univ. of Technology, Delft, The Netherlands 1994.
[8] P. Orlandi, M. Fatica, Direct simulations of turbulent flow in a pipe rotating about its axis, J. Fluid Mech. 343 (1997) 43–72.
[9] S. Imao, M. Itoh, T. Harada, Turbulent characteristics of the flow in an axially rotating pipe, Int. J. Heat Fluid Flow 17 (1996) 444–451.
[10] L. Facciolo, Experimental study of rotating pipe and jet flows, Licentiate thesis, KTH, Stockholm, Sweden, 2003, TRITA-MEK, 2003:15.
[11] M. Oberlack, Similarity in non-rotating and rotating turbulent pipe flows, J. Fluid Mech. 379 (1999) 1–22.
[12] S. Jakirlić, K. Hanjalić, A new approach to modelling near-wall turbulence energy and stress dissipation, J. Fluid Mech. 459 (2002) 139–166.
[13] O. Grundestam, S. Wallin, A.V. Johansson, A generalized EARSM based on a nonlinear pressure strain rate model, in: Proc. of the Third Conference on Turbulent Shear Flow Phenomena, TSFP-3, Sendai, Japan, June 2003.
[14] K. Alvelius, A.V. Johansson, Direct numerical simulation of rotating channel flow at various Reynolds numbers and rotation numbers, in doctoral thesis of K. Alvelius, Dept. of Mechanics, KTH, SE-100 44 Stockholm, 1999, TRITA- MEK Technical Report 1999:09, ISSN 0348-467X.
[15] D.C. Wilcox, Turbulence modeling for CFD, DCW Industries Inc., ISBN 0-9636051-0-0, USA, 1994.
[16] T. Sjögren, A.V. Johansson, Development and calibration of algebraic nonlinear models for terms in the Reynolds stress transport equations, Phys. Fluids 12 (2000) 1554–1572.

[17] B.J. Daly, F.H. Harlow, Transport equations in turbulence, Phys. Fluids 13 (1970) 2634–2649.
[18] W. Rodi, A new algebraic relation for calculating the Reynolds stresses, Z. Angew. Math. Mech. 56 (1976) 219–221.
[19] S. Wallin, A.V. Johansson, Modelling streamline curvature effects in explicit algebraic Reynolds stress turbulence models, Int. J. Heat Fluid Flow 23 (2002) 721–730.
[20] O. Grundestam, S. Wallin, A.V. Johansson, An explicit algebraic Reynolds stress model based on a nonlinear pressure strain rate model, Int. J. Heat Fluid Flow (2005), in press.
[21] S. Wallin, G. Mårtensson, A general 1D-solver for partial differential equations, in Licentiate thesis of G. Mårtensson, KTH, Stockholm, Sweden 2004, TRITA-MEK, Technical Report 2004:3.
[22] B. Lindgren, J.M. Österlund, A.V. Johansson, Evaluation of scaling laws derived from Lie group symmetry methods in zero-pressure-gradient turbulent boundary layers, J. Fluid Mech. 502 (2004) 127–152.
[23] M. Oberlack, A unified approach for symmetries in plane parallel turbulent shear flows, J. Fluid Mech. 427 (2001) 299–328.
[24] B.J. Cantwell, Introduction to Symmetry Analysis, Cambridge University Press, Cambridge, 2002.
[25] S.S. Girimaji, Fully-explicit and self-consistent algebraic Reynolds stress model, Theoret. Comput. Fluid Dyn. 8 (1996) 387–402.